$$\mathbf{E}^{c2}(\omega,t) = E_0(\hat{\mathbf{x}} - i\hat{\mathbf{y}})\cos\omega t,$$
$$\mathbf{j}_{c1}(\omega,t) = \sigma_{c1,c2}(\omega)\mathbf{E}^{c2*}(\omega,t) = \sigma_{c1,c2}(\omega)E_0(\hat{\mathbf{x}} + i\hat{\mathbf{y}})\cos\omega t, \tag{15}$$

where E_0 is the strength of the field. The absorption power at each circular polarization is then given by

$$W_a^{c1}(\omega) = \langle \mathbf{j}^{c2}(\omega,t)\cdot\mathbf{E}^{c1}(\omega,t)\rangle_t = \sigma_{c2,c1}(\omega)E_0^2,$$
$$W_a^{c2}(\omega) = \langle \mathbf{j}^{c1}(\omega,t)\cdot\mathbf{E}^{c2}(\omega,t)\rangle_t = \sigma_{c1,c2}(\omega)E_0^2, \tag{16}$$

where the time average gives $\langle\cos^2\omega t\rangle_t = 1/2$. On the other hand, the incident power of the light per unit cell area of each polarization is $W_i = c\,\varepsilon_0 E_0^2|\hat{\mathbf{x}} \pm i\hat{\mathbf{y}}|^2/2 = c\,\varepsilon_0 E_0^2$, so the difference in opacity for the two polarizations is $\mathcal{O}^{c1}(\omega) - \mathcal{O}^{c2}(\omega) = \left[W_a^{c1}(\omega) - W_a^{c2}(\omega)\right]/W_i$, which can be used to extract the Chern number spectral function and subsequently the Chern number by

$$\mathcal{C}^d(\omega) = \frac{1}{8\pi\omega}\left[\frac{\mathcal{O}^{c1}(\omega) - \mathcal{O}^{c2}(\omega)}{\pi\alpha}\right], \qquad \mathcal{C}^d = \int_0^\infty d\omega\,\mathcal{C}^d(\omega), \tag{17}$$

where $\alpha = e^2/4\pi c\,\varepsilon_0\hbar$ is the fine structure constant[29]. In other words, the Chern number spectral function can be simply extracted from the opacity difference between the two circular polarizations, similar to measurements in graphene[29, 30]. Moreover, because the finite temperature Chern number $\mathcal{C}^d$ is the frequency integrated spectral function, Eq. (17) implies that the opacity difference under circularly polarized light divided by frequency and then integrated over frequency must be a quantized integer at zero temperature, thereby realizing a topology induced frequency sum rule for noninteracting 2D materials [28]. This simple experimental protocol is easily accessible, thereby permitting a direct verification of the concepts proposed in our work.

We remark that the proper definition of Chern number at finite temperature has been contentious. Previous works based on linear response theory of DC Hall conductance suggest to define the finite temperature Chern number as the momentum-integration of the product of the Fermi distribution and the filled band Berry curvature $\sigma_{xy}^{DC} = \int \frac{d^2\mathbf{k}}{(2\pi)^2}\sum_n \Omega_{xy}^n f(\varepsilon_n^{\mathbf{k}})$, which is what measured in transport experiments[39, 40]. In contrast, our formalism based on optical Hall conductivity in Eq. (11) leads to an expression that contains the difference between the Fermi distributions of the filled bands and that of the empty bands, and a matrix element involving both filled and empty bands stemming from the optical absorption process. Thus our finite temperature formalism differs from that of the DC Hall conductance, and is specifically formulated to describe the opacity measurement of the Chern number at finite temperature.

2.3. Linear response theory of finite temperature Chern marker

The finite temperature Chern number can further be written into real space using the formalism in Sec. 2.1, yielding

$$\mathcal{C}^d = \frac{a^2}{\hbar^2}\int \frac{d^2\mathbf{k}}{(2\pi\hbar/a)^2}\sum_{\ell<\ell'}\left[i\langle\partial_x\ell|\ell'\rangle\langle\ell'|\partial_y\ell\rangle - (x\leftrightarrow y)\right]\left[f(\varepsilon_\ell^{\mathbf{k}}) - f(\varepsilon_{\ell'}^{\mathbf{k}})\right]$$

$$
\begin{aligned}
&= \frac{1}{a^2}\int \frac{d^2\mathbf{k}}{(2\pi\hbar/a)^2}\sum_{\ell<\ell'}\left[i\langle\psi_\ell^{\mathbf{k}}|\hat{x}|\psi_{\ell'}^{\mathbf{k}}\rangle\langle\psi_{\ell'}^{\mathbf{k}}|\hat{y}|\psi_\ell^{\mathbf{k}}\rangle - (x\leftrightarrow y)\right]\left[f(\varepsilon_\ell^{\mathbf{k}}) - f(\varepsilon_{\ell'}^{\mathbf{k}})\right] \\
&= \frac{1}{a^2}\int \frac{d^2\mathbf{k}}{(2\pi\hbar/a)^2}\int \frac{d^2\mathbf{k}'}{(2\pi\hbar/a)^2} \\
&\sum_{\ell<\ell'}\left[i\langle\psi_\ell^{\mathbf{k}}|\hat{x}|\psi_{\ell'}^{\mathbf{k}'}\rangle\langle\psi_{\ell'}^{\mathbf{k}'}|\hat{y}|\psi_\ell^{\mathbf{k}}\rangle - (x\leftrightarrow y)\right]\left[f(\varepsilon_\ell^{\mathbf{k}}) - f(\varepsilon_{\ell'}^{\mathbf{k}'})\right] \\
&= \frac{1}{Na^2}\sum_{\ell<\ell'}\left[i\langle E_\ell|\hat{x}|E_{\ell'}\rangle\langle E_{\ell'}|\hat{y}|E_\ell\rangle - (x\leftrightarrow y)\right]\left[f(E_\ell) - f(E_{\ell'})\right] \\
&= \frac{1}{Na^2}\sum_{\ell<\ell'}\mathrm{Tr}\left[i\hat{x}S_{\ell'}\hat{y}S_\ell - (x\leftrightarrow y)\right]\left[f(E_\ell) - f(E_{\ell'})\right], \qquad (18)
\end{aligned}
$$

where $|E_\ell\rangle$ is a lattice eigenstate obtained from diagonalizing the lattice Hamiltonian $H|E_\ell\rangle = E_\ell|E_\ell\rangle$, and we denote its projector by $S_\ell = |E_\ell\rangle\langle E_\ell|$. Here $|\psi_\ell^{\mathbf{k}}\rangle$ is the full Bloch state satisfying $\langle\mathbf{r}|\psi_\ell^{\mathbf{k}}\rangle = e^{i\mathbf{k}\cdot\mathbf{r}}\langle\mathbf{r}|\ell\rangle$, and in deriving Eq. (18) we have used

$$
\begin{aligned}
&\int \frac{d^2\mathbf{k}}{(2\pi\hbar/a)^2}|\psi_\ell^{\mathbf{k}}\rangle\langle\psi_\ell^{\mathbf{k}}| = \sum_\ell S_\ell, \\
&\int \frac{d^2\mathbf{k}}{(2\pi\hbar/a)^2}|\psi_\ell^{\mathbf{k}}\rangle\langle\psi_\ell^{\mathbf{k}}|f(\varepsilon_\ell^{\mathbf{k}}) = \sum_\ell S_\ell f(E_\ell), \qquad (19)
\end{aligned}
$$

At zero temperature, the Fermi distribution becomes a step function hence the indices $\ell \to n$ and $\ell' \to m$ are limited to the valence and conduction bands, respectively, so the Chern number in Eq. (18) recovers the zero temperature results in Eqs. (6) and (8).

However, from the discussion after Eq. (8), an extra projector analogous to P must be added to Eq. (18) in order to obtain the right Chern marker. The issue is then how should one consistently add a projector given that the thermal broadening at finite temperature renders the filled and empty states projectors P and Q in Eq. (7) rather ambiguous. For this purpose, we propose to first evaluate the matrix

$$
X = \sum_{\ell<\ell'} S_\ell \hat{x} S_{\ell'}\sqrt{f_{\ell\ell'}}, \qquad (20)
$$

and the analogous Y given by replacing $\hat{x} \to \hat{y}$, where $f_{\ell\ell'} \equiv f(E_\ell) - f(E_{\ell'})$. Having calculated these matrices, we define the finite temperature Chern marker by

$$
\mathcal{C}^d(\mathbf{r}) = \frac{i}{a^2}\langle\mathbf{r}|\left[X\,Y^\dagger - Y\,X^\dagger\right]|\mathbf{r}\rangle, \qquad (21)
$$

i.e., it is the diagonal element of the operator $i[X\,Y^\dagger - Y\,X^\dagger]$ that serves as the finite temperature generalization of the Chern operator defined after Eq. (8). The legitimacy of Eq. (21) relies on the fact that it encapsulates proper thermal broadening and spatially sums to the Chern number $\mathcal{C}^d = \sum_{\mathbf{r}}\mathcal{C}^d(\mathbf{r})/N$ in Eq. (18) since $\sum_{\mathbf{r}}|\mathbf{r}\rangle\langle\mathbf{r}| = I$ and $S_\ell S_{\bar{\ell}} = S_\ell\delta_{\ell\bar{\ell}}$. Essentially, our proposal is based on the assertion that the $\hat{P}\hat{x}\hat{Q}$ factor in Eq. (8) is generalized to the X operator in Eq. (20) at finite temperature in order to be consistent with our linear response theory of optical conductivity, i.e., the spatial sum of the Chern marker is proportional to the global Hall conductance.

Extending Eq. 20 to the frequency-dependent matrix

$$X(\omega) = \sum_{\ell<\ell'} S_\ell \hat{x} S_{\ell'} \sqrt{f_{\ell\ell'}\delta(\omega + E_\ell/\hbar - E_{\ell'}/\hbar)}, \tag{22}$$

(and the analogous $Y(\omega)$), a generalized Chern marker spectral function can now be extracted:

$$\mathcal{C}^d(\mathbf{r},\omega) = \mathrm{Re}\left[\frac{i}{a^2}\langle\mathbf{r}|\left[X(\omega)Y^\dagger(\omega) - Y(\omega)X^\dagger(\omega)\right]|\mathbf{r}\rangle\right]. \tag{23}$$

It is straightforward to see that $\mathcal{C}^d(\omega) = \sum_{\mathbf{r}} \mathcal{C}^d(\mathbf{r},\omega)/N$ (cf. Eq. (14)). Based on Sec. 2.2 we immediately conclude that the Chern marker spectral function represents the local opacity difference at the unit cell at $\mathbf{r}$:

$$\mathcal{C}^d(\mathbf{r},\omega) = \frac{1}{8\pi\omega}\left[\frac{\mathcal{O}^{c1}(\mathbf{r},\omega) - \mathcal{O}^{c2}(\mathbf{r},\omega)}{\pi\alpha}\right], \quad \mathcal{C}^d(\mathbf{r}) = \int_0^\infty d\omega\, \mathcal{C}^d(\mathbf{r},\omega). \tag{24}$$

The local opacity sums to the global one $\mathcal{O}^{c1}(\omega) = \sum_{\mathbf{r}} \mathcal{O}^{c1}(\mathbf{r},\omega)$. As a result, $\mathcal{C}^d(\mathbf{r},\omega)$ in principle can be detected by performing the opacity measurement described after Eq. (17) locally at $\mathbf{r}$. However, at zero temperature, one should keep in mind that $\mathcal{C}^d(\mathbf{r},\omega)$ is nonzero only at frequencies larger than the band gap of the material $\omega > \Delta$. Typical semiconducting band gaps $\Delta \sim$ eV likely necessitate circularly polarized light in the visible light range. As the wave lengths far exceed the lattice constant in this range, it will hinder the detection of local opacity in the nanometer scale. Nevertheless, we anticipate that $\mathcal{C}^d(\mathbf{r},\omega)$ may be detected by thermal probes such as scanning thermal microscopy[41, 42, 43, 44] that can detect the heating at the atomic scale caused by the circularly polarized light. The detected local absorption power $W_a^{c1}(\mathbf{r},\omega) - W_a^{c2}(\mathbf{r},\omega)$ then leads to Eq. (24) as a heating rate of the unit cell at $\mathbf{r}$.

3. Lattice model of Chern insulator

We now illustrate the power of the concepts described in the previous sections by exploring the concrete example of a prototypical 2D Chern insulator. The momentum space Hamiltonian in the basis $(c_{\mathbf{k}s},\ c_{\mathbf{k}p})^T$ is given by [45, 46]

$$\begin{aligned} H(\mathbf{k}) &= 2t\sin k_x \sigma^x + 2t\sin k_y \sigma^y \\ &+ \ (M + 4t' - 2t'\cos k_x - 2t'\cos k_y)\,\sigma^z. \end{aligned} \tag{25}$$

The internal degrees of freedom $\sigma = \{s, p\}$ are the orbitals. A straightforward Fourier transform leads to the two band lattice Hamiltonian [47]

$$\begin{aligned} H = &\sum_i t\left\{-ic_{is}^\dagger c_{i+ap} + ic_{i+as}^\dagger c_{ip} - c_{is}^\dagger c_{i+bp} + c_{i+bs}^\dagger c_{ip} + h.c.\right\} \\ &+ \sum_{i\delta} t'\left\{-c_{is}^\dagger c_{i+\delta s} + c_{ip}^\dagger c_{i+\delta p} + h.c.\right\} \\ &+ \sum_i (M + 4t')\left\{c_{is}^\dagger c_{is} - c_{ip}^\dagger c_{ip}\right\}, \end{aligned} \tag{26}$$

where $\delta = \{a, b\}$ represents the lattice constants in the two planar directions. Throughout the paper, we set $t = t' = 1.0$ and tune the mass term M to examine different topological phases, and the behavior of this model at finite temperature T. The model hosts topological phase transitions (TPT) at three critical points $M_c = \{-8, -4, 0\}$, reflecting gap closures at different high symmetry points (HSPs) in momentum space [48]. Since they all exhibit the same critical behavior [31, 32, 33], we will focus on the $M_c = 0$ critical point where the bulk gap closes at $\mathbf{k} = (0, 0)$.

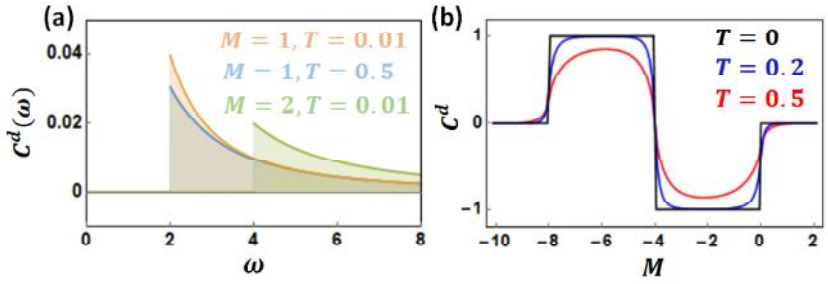

Figure 1. (a) The Chern number spectral function $\mathcal{C}^d(\omega)$ for the Chern insulator in a continuum, which is finite only at frequency larger than the bulk gap M, and moreover scales like $1/\omega^2$ such that it integrates to a finite value. The overall magnitude reduces with temperature. (b) The frequency-integrated Chern number $\mathcal{C}^d$ at zero and nonzero temperatures as a function of the mass term M.

Analytical results for this model can be obtained by linearizing the Hamiltonian near the HSP $\mathbf{k}_0 = (0, 0)$, yielding $E_{m,n} = \pm\sqrt{M^2 + v^2k^2}$ and a zero temperature Berry curvature $\Omega_{xy} = v^2M/2\left(M^2 + v^2k^2\right)^{3/2}$. The finite temperature Chern number spectral function in Eq. (14) is given by

$$\mathcal{C}^d(\omega) = \frac{M}{2\pi\hbar\omega^2}\left[f\left(-\frac{\hbar\omega}{2}\right) - f\left(\frac{\hbar\omega}{2}\right)\right]_{\omega\geq 2|M|/\hbar}. \tag{27}$$

At $T = 0$, $\mathcal{C}^d(\omega) \to \mathcal{C}(\omega)$ and is nonzero only if $\omega \geq 2|M|/\hbar$, since it represents an exciton absorption rate, as shown schematically in Fig. 1 (a). Moreover, the topological invariant $\mathcal{C} = \int_{2|M|/\hbar}^{\infty} d\omega\, \mathcal{C}(\omega) = \mathrm{Sgn}(M)/4\pi$. Essentially, this is the f-sum rule for exciton absorption rates in circular dichroism applied to topological insulators [28]. When $T \neq 0$, since the Fermi factor $f\left(-\frac{\omega}{2}\right) - f\left(\frac{\omega}{2}\right) \leq 1$, $\mathcal{C}^d < \mathrm{Sgn}(M)/4\pi$ is smaller than the quantized zero temperature Chern number, as illustrated in Fig. 1 (a). We anticipate that these predicted features should be readily verifiable by the opacity experiment proposed in Secs. 2.2.

The numerical results of the Chern number/marker $\mathcal{C}^d = \mathcal{C}^d(\mathbf{r})$ for the homogeneous lattice model of Chern insulator in Eq. (25) are shown in Fig. 1 (b). One sees that though the abrupt changes of the Chern number at the critical points are smeared out at nonzero temperature, clear vestiges of these TPTs are still present and should be observable in the experimentally accessible temperature range. To explain this smearing and examine the critical behavior, in Fig. 2 we present the evolution of the Chern number/marker

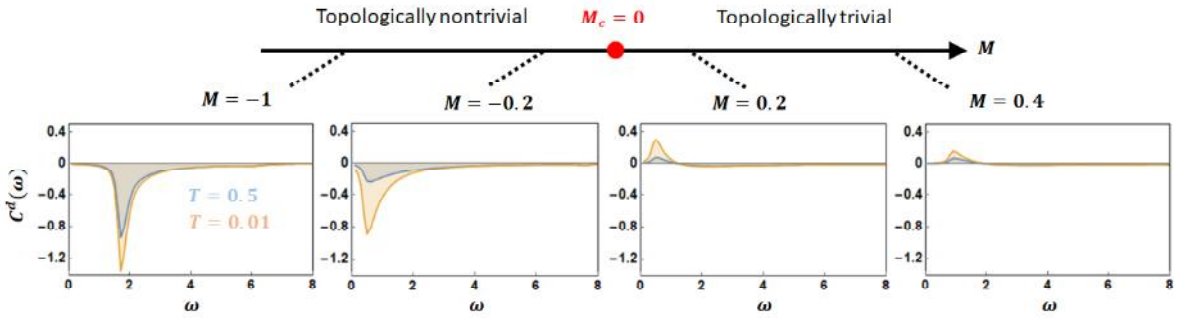

Figure 2. The Chern number spectral function $\mathcal{C}^d(\omega)$ for the lattice model of Chern insulator as a function of $M = \{-1, -0.2, 0.2, 0.4\}$ across the critical point $M_c = 0$, plotted for both low (orange) and high (blue) temperatures, where the δ-function in Eq. (27) is simulated by a Lorentzian with width $\eta = 0.1$. In the topologically nontrivial phase $M = \{-1, -0.2\}$, the spectral function is negative due to the negative Chern number $\mathcal{C}^d \approx -1$, and the spectral weight gradually shifts to low frequency as $M \to M_c$. In the topologically trivial phase $M = \{0.2, 0.4\}$ and at low temperature, the positive and negative regions together yield $\mathcal{C}^d \approx 0$ (up to numerical precision).

spectral function $\mathcal{C}^d(\omega) = \mathcal{C}^d(\mathbf{r}, \omega)$ across the critical point M_c at both low and high temperatures. In the topologically nontrivial phase $M < 0$, the spectral function is negative (consistent with $\mathcal{C} = -1$) and the magnitude is largest near the band gap $\omega \approx 2|M|$, reflecting that excitations of states in the vicinity of the band gap are the most detrimental to the topological properties of the system. The role of temperature is to reduce the overall magnitude of the spectral function and subsequently the frequency integration, consistent with the smearing presented in Fig. 1 (b). On the other hand, in the topologically trivial phase $M > 0$, the spectral weight has both positive and negative components such that it integrates to a zero Chern number $\mathcal{C}^d \approx 0$ at low temperature. Interestingly, the effect of temperature is to reduce the positive peak at low frequency and make the overall frequency integration slightly negative, which explains the smearing of the sharp jump of $\mathcal{C}^d$ at the critical point by temperature as shown in Fig. 1 (b). Comparing the $M = -0.2$ and $M = 0.2$ panels in Fig. 2, we see that the spectral weight near the band gap flips sign as the system crosses the TPT at $M_c = 0$, in accordance with the flipping of Berry curvature at the HSP $\mathbf{k}_0 = (0, 0)$, a defining feature of TPTs [49, 31, 32, 33]. Interestingly, these features of $\mathcal{C}^d(\omega)$ bear a striking similarity with the Haldane-type Floquet topological insulator[22]. The latter has been realized in cold atoms that has an extremely narrow band width $\sim 10^{-12}$eV, in which the zero temperature limit of $\lim_{T\to 0} \mathcal{C}^d(\omega)$ hs been measured. This indicates that these features may be generic indicating that these features may be generic for Chern insulators realized in a variety of different energy scales.

Finally, combining the shape of $\mathcal{C}^d(\omega)$ in Fig. 2 with the opacity measurement proposed in Sec. 2.2 implies a remarkably simple way to infer the finite temperature Chern number in 2D materials. Figure 2 suggests that if a 2D material always appears more transparent under right circularly polarized light than the left (or vice versa) at any

frequency, then the material must be topologically nontrivial, as $\mathcal{C}^d(\omega)$ is always of the same sign and hence it must frequency-integrate to a finite Chern number. Depending on the frequency range of $\mathcal{C}^d(\omega)$ in real materials, this should be directly visible to the naked eye or through an infrared/UV lens, offering a very simple way to perceive the topological order in the macroscopic scale. On the other hand, if the transparency of the material under the two circular polarizations is strongly frequency dependent, then a frequency integration of $\mathcal{C}^d(\omega)$ is required to infer the Chern number.

4. Topological quantum criticality

The Chern marker is known to display interesting critical behavior near TPTs, such as size-dependent smoothening of its discontinuity [50], Kibble-Zurek scaling in disordered Chern insulators [51], and Hofstadter-butterfly-like features in quasicrystals [52]. As with standard symmetry breaking critical points, where correlation functions of the order parameter show divergent correlation lengths, here, using linear response theory, we explore if there exist certain nonlocal correlators that will display such singular behavior near TPTs. We identify two quantities: a *Chern correlator* and a *nonlocal Chern marker*, which encode different physics pertaining to the topological quantum criticality.

4.1. Chern correlator

Based on the linear response theory presented earlier, we define a Chern correlator spectral function by splitting the second position operator $\hat{x} = \sum_{\mathbf{r}'} \hat{x}_{\mathbf{r}'}$ in Eq. (23) into its component on each site $\mathbf{r}'$, yielding

$$\begin{aligned}
\tilde{\mathcal{C}}(\mathbf{r},\mathbf{r}',\omega) &= \mathrm{Re}\left[\frac{i}{a^2}\langle\mathbf{r}|\left[X(\omega)Y^\dagger_{\mathbf{r}'}(\omega) - Y(\omega)X^\dagger_{\mathbf{r}'}(\omega)\right]|\mathbf{r}\rangle\right], \\
X^\dagger_{\mathbf{r}'}(\omega) &= \sum_{\ell<\ell'} S_{\ell'}\hat{x}_{\mathbf{r}'}S_\ell\sqrt{f_{\ell\ell'}\delta(\omega+E_\ell/\hbar-E_{\ell'}/\hbar)},
\end{aligned} \tag{28}$$

which spatially sums to the Chern marker spectra function $\mathcal{C}^d(\mathbf{r},\omega) = \sum_{\mathbf{r}'}\tilde{\mathcal{C}}(\mathbf{r},\mathbf{r}',\omega)$ in Eq. (23). This splitting of the second position operator is justified by the observation that in Eqs. (11) and (18), the second position operator accounts for the global field. Consequently, this Chern correlator spectral function $\tilde{\mathcal{C}}(\mathbf{r},\mathbf{r}',\omega)$ represents the local current at site $\mathbf{r}$ caused by applying a field of frequency ω at site $\mathbf{r}'$, i.e., the nonlocal current response. A frequency integration $\tilde{\mathcal{C}}(\mathbf{r},\mathbf{r}') = \int_0^\infty d\omega\,\tilde{\mathcal{C}}(\mathbf{r},\mathbf{r}',\omega)$ further leads to a Chern correlator

$$\begin{aligned}
\tilde{\mathcal{C}}(\mathbf{r},\mathbf{r}') &= \mathrm{Re}\left[\frac{i}{a^2}\langle\mathbf{r}|\left[X\,Y^\dagger_{\mathbf{r}'} - Y\,X^\dagger_{\mathbf{r}'}\right]|\mathbf{r}\rangle\right], \\
X^\dagger_{\mathbf{r}'}(\omega) &= \sum_{\ell<\ell'} S_{\ell'}\hat{x}_{\mathbf{r}'}S_\ell\sqrt{f_{\ell\ell'}}
\end{aligned} \tag{29}$$

This correlator sums to the Chern marker $\sum_{\mathbf{r}'}\tilde{\mathcal{C}}(\mathbf{r},\mathbf{r}') = \mathcal{C}^d(\mathbf{r})$ and represents a measure of the internal fluctuation of the Chern marker. Note that in a clean and infinite